Journal of Alloys and Compounds 669 (2016) 117–122

Contents lists available at ScienceDirect

Journal of Alloys and Compounds

journal homepage: http://www.elsevier.com/locate/jalcom

Effect of dose and post irradiation annealing in Ni implanted high entropy alloy *FeCrCoNi* using slow positron beam

S. Abhaya*, R. Rajaraman, S. Kalavathi, C. David, B.K. Panigrahi, G. Amarendra

Materials Science Group, Indira Gandhi Centre for Atomic Research, Kalpakkam 603 102, India

ARTICLE INFO

Article history:
Received 24 November 2015
Received in revised form
29 January 2016
Accepted 29 January 2016
Available online 2 February 2016

Keywords:
High entropy alloy
Radiation damage
X-ray diffraction
Positron annihilation spectroscopy

ABSTRACT

Defect characterization of room temperature 1.5 MeV Ni ion implanted high entropy *FeCrCoNi* alloy for two fluences (1×10^{15} ions/cm^2 and 5×10^{16} ions/cm^2) was carried out using the variable low energy positron beam. The FCC solid solution remains robust and stable under 100 dpa irradiation and high temperature annealing. The change in the defect sensitive S-parameter upon implantation reveals the presence of monovacancies for both the doses. The changes in the defect microstructure upon thermal annealing are found to be dose dependent. The high dose shows the formation of stable stacking fault tetrahedrons (SFT's) from the aggregates of monovacancies at higher annealing temperatures while the low dose shows the annealing of monovacancies with temperature.

© 2016 Elsevier B.V. All rights reserved.

1. Introduction

High entropy alloys (HEA) are multicomponent alloys in which the elements present are in equiatomic or near equiatomic proportions [1–5]. Due to the presence of multiple elements in near equiatomic proportions, the configurational entropy increases resulting in the formation of simple solid solutions. High entropy alloys exhibit excellent properties such as high strength, high temperature resistance, good corrosion and oxidation resistance and therefore are the potential candidates for high temperature structural applications in nuclear reactors [6]. To be used as a structural material in advanced nuclear reactors, it is important to know the phase stability as well as the defect microstructure in these alloys under high irradiation doses, high temperature and extremely corrosive environments. It is of interest to know how the multicomponent nature of the high entropy alloy would affect the system under severe irradiation conditions-the nature of the displacement cascades produced and whether the number of survived vacancies and interstitials at the end of the displacement cascades would be different from that of the conventional austenitic steels. Recently, a number of papers have been published dealing with the post irradiation analysis on various HEA's using a variety of techniques, namely, HRTEM (high resolution transmission electron microcopy) along with SAD (selected area diffraction) to reveal the microstructures, dislocation loops, voids etc., AFM (atomic force microscopy) to characterize the swelling behaviour, nano-indentation to measure the hardness, stress–-strain curves to measure the elastic modulus, yield strength, ductility and rupture, scanning transmission electron microscopy (STEM) to look for possible radiation induced segregation of elements at the grain boundaries as a function of energy of ions/electrons, dose and irradiation temperature [7–9]. In particular, Peter K. Liaw et al. [7], studied the microstructural evolution upon irradiation of 5 MeV Ni on $Al_{0.3}CoCrFeNi$ using TEM and AFM. The findings showed good phase stability and good swelling resistance i.e., no voids or dislocations up to 60 peak dpa. In line with this observation, C. Li et al. [8], reported the presence of dislocation loops and absence of void formation in $FeNiMnCr_{18}$ for 5.8 MeV Ni^{2+} ions irradiated with a dose range of 1–10 dpa and temperature range 400–700 °C and also that only a small fraction of the produced point defects are trapped in the loops and the rest of point defects eventually recombine making the HEA highly resistant to swelling. Kiran Kumar et al. [9], reported that the Fe–28%Ni–27% Mn–18%Cr high entropy alloy showed no voids when irradiated with 3 MeV Ni^{2+} for 10 dpa at 500 °C unlike the conventional Fe–Cr–Ni austenitic steel which shows the presence of voids at 500 °C.

Positron annihilation spectroscopy [10] is a unique defect characterization technique to study irradiation induced defects such as vacancies and voids in materials. Positrons are sensitive and

* Corresponding author.
E-mail address: sab@igcar.gov.in (S. Abhaya).

http://dx.doi.org/10.1016/j.jallcom.2016.01.242
0925-8388/© 2016 Elsevier B.V. All rights reserved.

selective to vacancy defects and can probe starting from single vacancy to vacancy clusters in materials up to a depth of a few hundreds of microns. With positron beam, depth resolved defect studies can be carried out from near surface up to a depth of a few hundreds of nm [11]. The present paper reports for the first time, the study of Ni implantation induced defects in *FeCrCoNi* alloy and the evolution of the defect microstructure with thermal annealing and its dose dependence using the variable low energy positron beam.

2. Experimental details

Stoichiometric proportions of 99.99+% pure Fe, 99.99+% pure Cr, 99.999% pure Ni (all from M/s GoodFellow) and 99.9+% pure Co (M/s Alfa Aesar) were taken. The alloy preparation and the alloy composition is given elsewhere [12]. The arc melted button was cut into two pieces and annealed at 1100 K for 4 h to obtain a defect free alloy. The two well annealed *FeCrCoNi* samples of diameter 10 mm and thickness 1 mm were then subsequently implanted with 1.5 MeV Ni ions using the 1.7 MV Tandetron accelerator to a fluence of 1×10^{15} (low dose) and 5×10^{16} (high dose) ions/cm^2 at room temperature. Depth resolved Doppler broadening measurements were carried out on these samples annealed in the temperature range 300–1173 K using the variable low energy positron beam [13]. The positron beam energy was varied from 0 to 20 keV in steps of 0.5 keV. For each positron beam energy, the annihilation spectrum was monitored using the HPGe detector of 30% efficiency and having resolution of 1.5 keV for Cs^{137} ray. Both S-parameter and W-parameter were deduced from the annihilation spectrum for each positron beam energy. The S-parameter characterizes the annihilation of positrons with the valence electrons and therefore an increase in S-parameter with respect to that obtained for a defect free sample implies the presence of vacancy defects. The W-parameter characterizes the annihilation of positrons with the core electrons and is therefore sensitive to the chemical nature at the annihilation site. The ratio of S-parameter to W-parameter is given by a defect specific R-parameter. The R-parameter depends only on the nature of defects and not on its concentration [10,11,14,15]. Therefore, any change in the nature of defects can be probed by the R-parameter. Theoretical positron lifetime of *FeCrCoNi* was obtained using the DOPPLER code [16] which uses the atomic superposition method. Glancing incidence X-ray diffraction measurements (GIXRD) were performed on the implanted sample and also after isochronal annealing of the specimen at selected temperatures for both the doses to follow the structural stability of the alloy. The measurements were carried out using a STOE make powder diffractometer at a glancing incidence of 0.5° with Cu k_α radiation ($\lambda = 1.5406$ Å). The diffraction data were collected with a step size of 0.1° from 20° to 95° using a scintillation detector.

3. Results and discussion

Fig. 1 shows the ion distribution profile as well as the vacancy distribution profile for 1.5 MeV Ni ion implanted *FeCrCoNi* as deduced from SRIM code [17]. The figure shows the ion distribution from the near surface up to a depth of 800 nm with a maximum centered around 500 nm, while the damage depth starts from near surface and peaks at around 400 nm and tapers off beyond 800 nm. This damage depth is well within the depth probed by the positron beam which is approximately 840 nm for a positron beam energy of 21 keV.

GIXRD characterization on Ni ion implanted *FeCrCoNi* reveals FCC structure [18]. The structure remains stable under both implantation and annealing at temperatures as high as 1173 K as shown in Fig. 2.

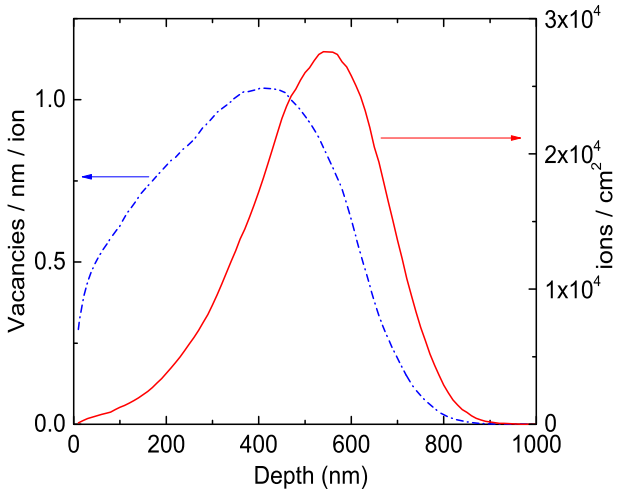

Fig. 1. Vacancy distribution (dashed line) and Ni ion distribution (solid line) for 1.5 MeV Ni ion implanted *FeCrCoNi* at room temperature using SRIM [17].

The calculated peak damage in terms of the displacement per atom (dpa) for 1.5 MeV Ni ion implanted *FeCrCoNi* amounts to 2 and 96 dpa for the fluences 1×10^{15} ions/cm^2 and 5×10^{16} ions/cm^2, respectively. In order to understand the damage behaviour in *FeCrCoNi* implanted with Ni ions, Doppler S-parameter based positron beam measurements on both low dose (10^{15} ions/cm^2) and high dose (5×10^{16} ions/cm^2) samples were carried out as a function of annealing temperature. Figs. 3 and 4 show the Doppler S-parameter as a function of positron beam energy (E_p) at different annealing temperatures for low and high dose samples, respectively. The positron beam based S-parameter behaviour as a function of positron beam energy is as follows. For the defect free *FeCrCoNi*, the S-parameter is high at the surface, it then decreases and saturates at 0.49 beyond 16 keV. This trend is typical of any metal wherein the electron density is low at the surface giving a high S-parameter value and as the positron beam probes deeper depths, the electron density becomes high giving a low S-parameter. The value of 0.49 (S_b) corresponds to positron annihilation from the defect free state. For the Ni implanted *FeCrCoNi*, the S-

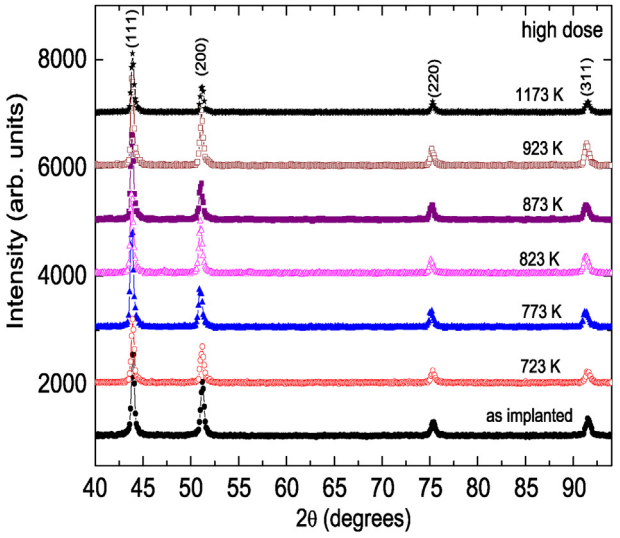

Fig. 2. GIXRD spectra for FeCrCoNi implanted with 1.5 MeV Ni ions to a fluence of 5×10^{16} ions/cm^2 (high dose) annealed at different temperatures as a function of post-implantation annealing. The peaks are indexed.

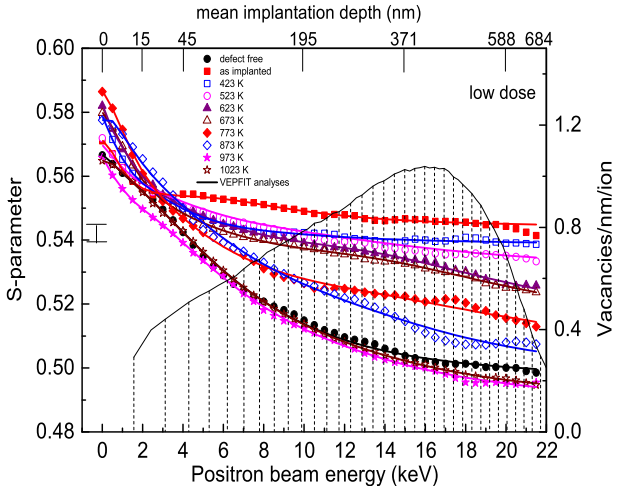

Fig. 3. Variation of Doppler S-parameter with positron beam energy for *FeCrCoNi* implanted with 1.5 MeV Ni ions to a fluence of 10^{15} ions/cm^2 annealed at different temperatures. The mean implantation depth is shown on the top axis. S vs. E_p curves for alternate temperatures are skipped for better clarity. The SRIM profile is also inserted to show the damage depth probed by the positron beam. The solid lines through the data points are a result of VEPFIT analyses.

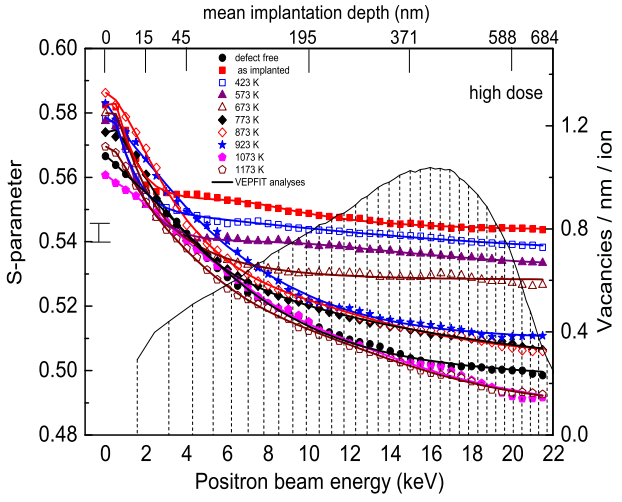

Fig. 4. Variation of Doppler S-parameter with positron beam energy for *FeCrCoNi* implanted with 1.5 MeV Ni ions to a fluence of 5×10^{16} ions/cm^2 annealed at different temperatures. The mean implantation depth is shown on the top axis. S vs. E_p curves for alternate temperatures are skipped for better clarity. The SRIM profile is also inserted to show the damage depth probed by the positron beam. The solid lines through the data points are a result of VEPFIT analyses.

parameter is high at the surface (for $E_p < 1$ keV) and then decreases and saturates beyond 3 keV at 0.542. The high saturation S-parameter of 0.542 (S_d) beyond 3 keV corresponds to positron annihilation in implantation induced vacancy defects in *FeCrCoNi* for the low dose. It is interesting to note that the same trend is followed for the high dose sample i.e., the S-parameter is high for low E_p and then it decreases and saturates to 0.542 beyond 3 keV. It is evident that there is saturation trapping of positrons for both the low as well as the high dose samples. A normalized S-parameter (given by $S_d/S_b = 0.542/0.49$) of 1.10 is obtained for both the doses. It is reported that for positrons annihilating from the monovacancy trapped states in nickel, the normalized S-parameter is 1.11 [19]. This value compares well with that obtained for Ni implantation in *FeCrCoNi* indicating that the defects are monovacancies. In order to understand the defect recovery process in both high and low dose samples, positron beam measurements were carried out and S vs. E_p curves for both high and low dose samples exposed to different annealing temperatures were obtained. It is observed from Figs. 3 and 4, that at higher annealing temperatures, the saturation S-parameter slowly decreases from 0.542 to 0.49 (defect-free) and the S vs. E_p curve matches with that of the defect free *FeCrCoNi* for annealing temperatures beyond 923 K for the low dose and 1073 K for the high dose samples, respectively.

Based on the above observations two points can be inferred, namely, a) irrespective of the dose, both the samples show saturation trapping of positrons beyond 3 keV and b) the defect type in both the doses are monovacancies and there is no evidence of vacancy clustering.

In order to follow the annealing of monovacancies in both the doses, VEPFIT analyses [20] was done and the experimental S vs. E_p curves were fitted. For the high dose, a two layer fitting comprising of a near surface layer and an extended defect layer was done. While for the low dose, a three layer fitting comprising of a near surface layer, highly defected layer and an extended defect layer was done. For the high dose, the S vs. E_p curves show a flat behaviour at deeper depths even at higher annealing temperatures, while for the low dose, the S vs. E_p curves show a slope at deeper depths. This slope could be accounted for only by a three layer fitting. While for the high dose, a simple two layer fitting would suffice. A plausible reason for the trend of S vs. E_p curves could be attributed to the defect concentration. Because of the higher defect concentration in the high dose, annealing of defects in to the bulk during the defect recovery process is not that evident. This produces a flat behaviour in the S vs. E_p for deeper depths even at higher annealing temperatures. While for the low dose having comparatively less defect concentration, the annealing of defects in to the bulk is evident showing an effective contribution of positron annihilation from the bulk. This produces a slope at deeper depths for the low dose. The VEPFIT deduced S-parameter values corresponding to all these layers as a function of annealing temperature for both the doses were obtained. Fig. 5 shows the VEPFIT S-parameter of the defected layer for both the doses as a function of annealing temperature. For the low dose, the S-parameter corresponding to the highly defected layer and the extended defect layer were averaged and then plotted in Fig. 5. Interestingly, from VEPFIT analyses for the low dose, the defect volume probed by the positron

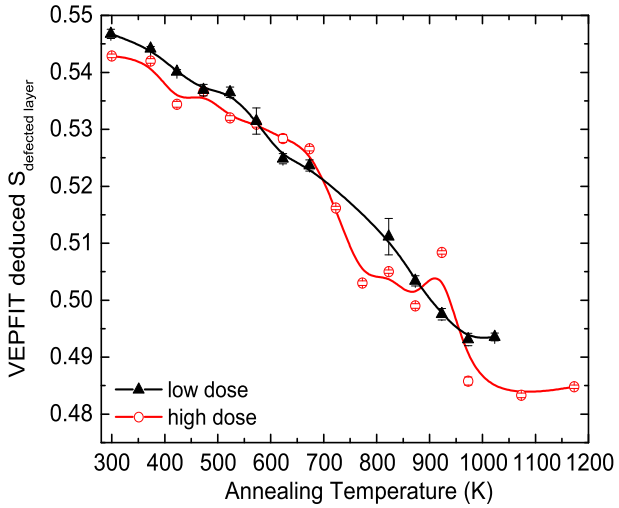

Fig. 5. Variation of VEPFIT deduced S-parameter corresponding to the defected layer as a function of annealing temperature for both low and high doses.

shrinks at higher temperatures. As seen in Fig. 5, for the high dose sample, there are two distinct recovery stages, one in the temperature range 300–723 K and other in the temperature range 773–923 K and there is complete annealing of defects beyond 973 K. But in the low dose, the second recovery stage is not evident. There is complete annealing of defects beyond 973 K for the low dose.

Figs. 6 and 7 show the S–W plot for the low and the high doses, respectively. Both the doses show a linear decrease in (S, W) with temperature indicating the annealing of defects in the samples. But the defect specific R-parameter obtained for both the doses are not the same. This indicates that the nature of defects evolved with thermal treatment are not the same even though monovacancies are produced in the as implanted condition for both the doses. It is observed from Figs. 6 and 7 that $R_{lowdose} > R_{highdose}$. It may be pointed out that $R_{lowdose}$ is comparable to that in electron irradiated nickel which is 1.56 ± 0.05 [19] confirming that the positron trapping sites are monovacancies and there is annealing of these defects with temperature for the low dose. For the high dose, apart from the annealing of monovacancies, there is an evolution of another defect type making the R-parameter lower in high dose when compared to low dose.

M. Eldrup et al. [21], have reported that for room temperature irradiation in FCC metals like copper or nickel, monovacancies and or very small vacancy clusters known as stacking fault tetrahedra (SFT's) are formed and void nucleation is not observed below the recovery stage V (typically around 573 K) while in BCC metal like iron, microvoids are formed at room temperature (just above stage III). The FCC structure of *FeCrCoNi* is a key factor for the formation of SFT's. Another key parameter for the formation and stability of SFT's is the low stacking fault energy. It may be recalled that our recent positron lifetime measurements on arc melted *FeCrCoNi* showed a delay in the defect recovery with annealing temperature when compared to cold worked Fe or Ni and this delay was attributed to the low stacking fault energy arising due to the multiple elements present in the alloy [12]. From GIXRD measurements, the stacking fault probability (α) can be deduced from the shift differences between the (111) and the (200) lines according to the relation

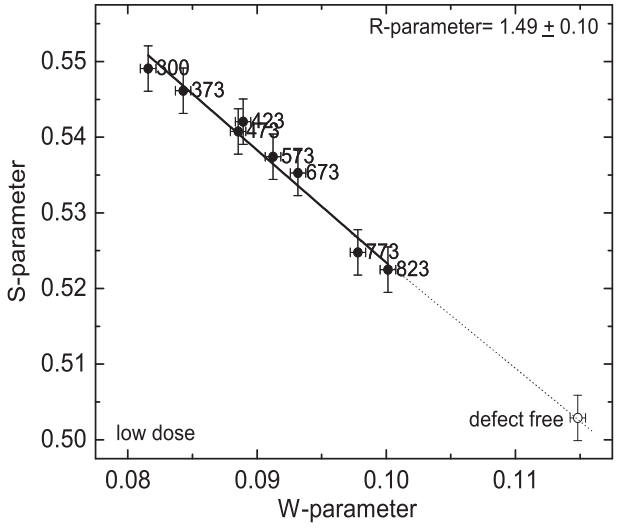

Fig. 6. S–W correlation plot for the low dose. The line joining the data points is a guide to the eye. The extrapolated dotted line exactly passes through the defect free (S, W) point.

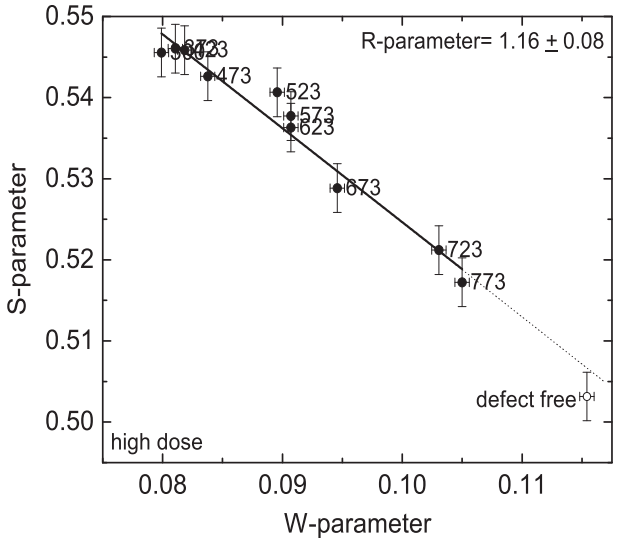

Fig. 7. S–W correlation plot for the high dose. The line joining the data points is a guide to the eye. The extrapolated dotted line falls above the defect free (S, W) point.

$$\alpha = -\pi^2 \Delta(2\theta_{200} - 2\theta_{111}) \Big/ 45\sqrt{3}(\tan\theta_{200} + 0.5\tan\theta_{111}) \qquad (1)$$

where, $\Delta(2\theta_{200} - 2\theta_{111})$ is calculated based on the difference of $\Delta 2\theta_{200} = 2\theta_{200} - 2\theta^o_{200}$ and $\Delta 2\theta_{111} = 2\theta_{111} - 2\theta^o_{111}$ where $2\theta^o_{200}$ and $2\theta^o_{111}$ are the (111) and (200) peak positions in a sample without faults [22].

Fig. 8 shows the variation of stacking fault probability (α) with annealing temperature. It may be noted that α is negligible for the as implanted condition of both doses. GIXRD measurements were done beyond 600 K annealing and hence the behaviour at lower annealing temperatures could not be followed. Stacking fault probability is negligible throughout the annealing for low dose sample. However for the high dose, it showed high value at 723 K and then decreased beyond 873 K. It is known that the stacking fault energy is inversely proportional to the stacking fault probability for a given dislocation density and shear modulus [22]. This means that in the temperature range of 700–873 K for the high

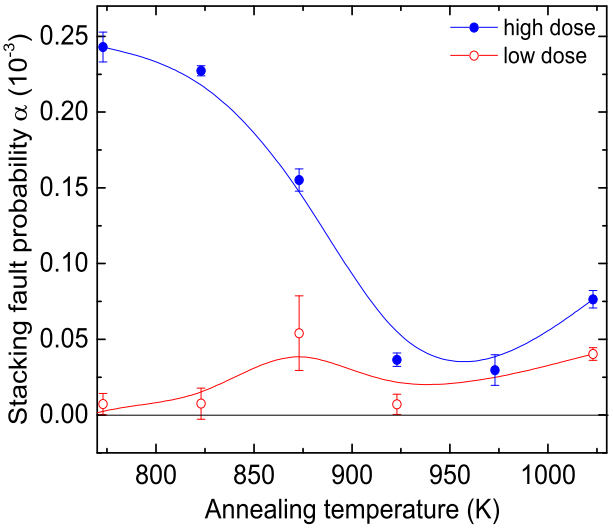

Fig. 8. Variation of stacking fault probability (α) with temperature for *FeCrCoNi* corresponding to both the doses.

dose, the probability of forming stacking fault tetrahedra is high indicating that the stacking fault energy is minimum. This also suggests that SFT's are not formed in the low dose sample while in high dose sample, the SFT's are formed beyond 700 K and are stable up to 823 K. Therefore, the second recovery stage observed in the S vs. T (Fig. 5) in the temperature range 700–923 K is attributed to the formation of stable SFT's for the high dose. For higher annealing temperatures, the SFT's collapse and vacancies are annealed out completely. Kuhlmann-Wilsdorf et al. [23], have reported that during irradiation and post-irradiation annealing, the SFT's grow in size but beyond a certain critical size of 6–8 nm, the SFT becomes less energetically favourable and collapses in to vacancy loops which then shrink by vacancy emission. Kuramoto et al. [24], have performed positron lifetime calculations on relaxed SFT structures in Ni and the positron lifetime varies from 170 ps for SFT's containing 6 vacancies to 130 ps containing 28 vacancies. Therefore, smaller the size of SFT's, larger is the positron lifetime and the lifetime is less than that of a monovacancy. As the SFT's grow bigger in size, the positron lifetime decreases. This suggests that the annealing of monovacancies together with the formation of stable SFT's makes the $R_{highdose}$ lower than that of $R_{lowdose}$. More recently, Aidhy et al. [25], have reported using molecular dynamics the formation of SFT's from mere aggregates of monovacancies for randomly located Frenkel pairs in a randomly distributed binary alloy of equiatomic NiFe and NiCr. The above mechanism for the formation of SFT's supports the present results in the sense that for the high dose sample, monovacancies are formed in the as implanted condition and with thermal treatment, the monovacancies aggregate to form stable SFT's which then collapse at higher temperatures. The current positron beam result also points out that no microvoids are produced.

It is of interest to find out the theoretical positron lifetime corresponding to a SFT in this alloy. Towards this, a $5 \times 5 \times 5$ FCC super cell of equiatomic *FeCrCoNi* was constructed. Along the (111) plane, a triangular platelet of vacancies were removed and the rest of the atoms below the platelet were displaced by $a_0/\sqrt{3}$ (a_0 is the lattice parameter). This is to actually create a stacking fault. The resultant super cell was given as input to the DOPPLER code [16] and the positron lifetime for the unrelaxed configuration was obtained. The positron lifetime for the defect free *FeCrCoNi* was deduced to be 101 ps and for that containing monovacancy was 170 ps. In the case of SFT containing 28, 45, 79 vacancies, the positron lifetime remained constant at 192 ps. Fig. 9 shows the positron density distribution in the XY plane for a SFT containing 28 vacancies using XCRYSDEN [26]. It is observed that the positron density is maximum at the apex rather than at the base of the pyramid.

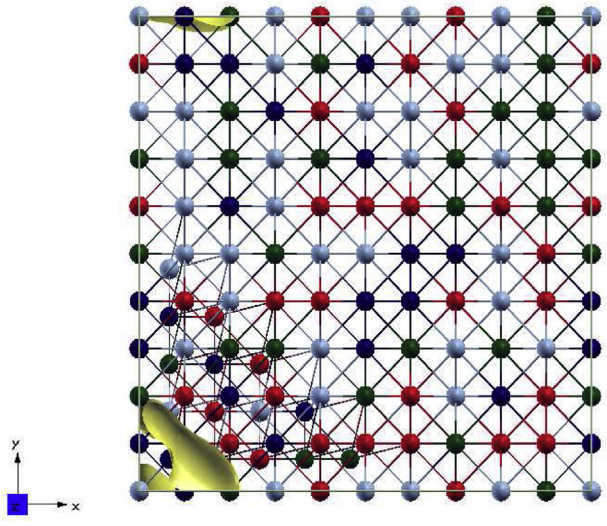

Fig. 9. Positron density distribution (shown in yellow) in XY plane for an SFT containing 28 vacancies in $5 \times 5 \times 5$ super cell of *FeCrCoNi* alloy. Cr atoms are shown in light blue, Fe in red, Co in green and Ni in dark blue.

The absence of microvoid formation in the current investigation is argued in the following way: a) The excess vacancies and interstitials at the end of displacement cascade recombine effectively due to the multicomponent nature of the alloy showing no void formation [8,9]. b) The atomic level stresses due to the atomic size difference in HEA are so high in the system that amorphization takes place subsequent to ion irradiation. There is amorphous to crystalline transition due to energy deposition leaving behind less defects in the system preventing void swelling behaviour when compared to conventional austenitic steels [27–29]. Our present work shows that the *FeCrCoNi* is structurally stable under both high irradiation (~100 dpa) and high temperature annealing and also, it is observed that only SFT's are formed and no microvoids are formed in as implanted condition as well as under thermal annealing. This makes high entropy alloys as potential candidates for application in nuclear reactor as structural materials.

4. Conclusions

Microstructural evolution of defects and defect recovery in Ni ion implanted high entropy *FeCrCoNi* alloy upon post irradiation annealing was studied using the positron beam. It is observed that irrespective of the dose, the S vs E_p curves of the as implanted sample show a saturation behaviour. The value of the normalized S-parameter suggests the presence of monovacancies for both the doses. Post irradiation annealing of the implanted sample for the high dose shows a second defect recovery stage.

This stage, in the temperature range of 700–823 K, is attributed to the presence of SFT's formed from mere aggregates of monovacancies. The stacking fault probability obtained from the GIXRD peak positions supports the formation of SFT's corresponding to the second recovery stage. At higher annealing temperatures, the SFT's collapse and the vacancies anneal out. Absence of formation of SFT's for low dose irradiation implies that there is a dose dependence for the formation of SFT's. From the application point of view, this alloy does not show microvoid formation even under doses as high as 100 dpa and high annealing temperatures unlike the conventional austenitic stainless steels.

Acknowledgements

The authors gratefully acknowledge Mr. L. Meenakshi Sundaram for synthesizing the alloy using arc melting technique.

References

[1] J.W. Yeh, S.K. Chen, S.J. Lin, J.Y. Gan, T.S. Chin, T.T. Shun, C.H. Tsai, S.Y. Chang, Adv. Eng. Mater. 6 (2004) 299.
[2] J.W. Yeh, Y.L. Chen, S.J. Lin, S.K. Chen, Mater. Sci. Forum 560 (2007) 1.
[3] Jien-Wei Yeh, J. Miner. Metals Mater. Soc. 65 (2013) 1759.
[4] Ming-Hung Tsai, Jien-Wei Yeh, Mater. Res. Lett. 2 (2014) 107.
[5] Yong Zhang, Ting Ting Zuo, Zhi Tang, Michael C. Gao, Karin A. Dahmen, Peter K. Liaw, Zhao Ping Lu, Prog. Mater. Sci. 61 (2014) 1.
[6] Daniel B. Miracle, Jonathan D. Miller, Oleg N. Senkov, Christopher Woodward, Michael D. Uchic, Jaimie Tiley, Entropy 16 (2014) 494.
[7] Peter K. Liaw, Takeshi Egami, Chuan Zhang, Fan Zhang, and Yanwen Zhang, Wei Guo, Yuting Li, Lou Santodonato, and Zhi Tang, Project No. 11–3196, NEUP, U.S Dept. of Energy.
[8] C. Li, S. J. Zinkle, N.A.P. Kiran Kumar, H. Bei, DOE/ER-0313/54-Volume 5, June 30, 2013.
[9] N. A. P. Kiran Kumar, K. J. Leonard, H. Bei, T. S. Byun, Y. Zhang and S. J. Zinkle, DOE/ER-0313/54-Volume 5, June 30, 2013.
[10] W. Brandt, A. Dupasquier, Positron Solid State Physics, North-Holland,

Amsterdam, 1982.
[11] P.J. Schultz, K.G. Lynn, Rev. Mod. Phys. 60 (1988) 701.
[12] S. Abhaya, R. Rajaraman, S. Kalavathi, G. Amarendra, J. Alloys Compd. 620 (2015) 277–282.
[13] G. Amarendra, B. Viswanathan, G. Venugopal Rao, J. Parimala, B. Purniah, Curr. Sci. 73 (1997) 409.
[14] R. Krause-Rehberg, H.S. Leipner, Positron Annihilation in Semiconductors, Springer Verlag, Berlin, 1998.
[15] K. Saarinen, P. Hautojarvi, C. Corbel, in: M. Stavola (Ed.), Identification of Defects in Semiconductors, Academic Press, New York, 1998.
[16] T. Torsti, M. Heiskanen, M.J. Puska, R.M. Nieminen, Int. J. Quantum Chem. 91 (2003) 171.
[17] J.F. Ziegler, J.P. Biersack, U. Littmark, The Stopping and Range of Ions in Solids, Pergamon Press, New York, 2003.
[18] Y.J. Hsu, W.C. Chang, J.K. Wu, Mater. Chem. Phys. 92 (2005) 112.
[19] A.P. Druzhkov, A.L. Arbuzov, D.A. Perminov, J. Nucl. Mater. 421 (2012) 58.
[20] A. Van Veen, H. Schut, J. de Vries, R.A. Hakvoort, M.R. Ijpma, AIP Conf. Proc. 218 (1990) 171.
[21] M. Eldrup, B.N. Singh, J. Nucl. Mater. 276 (2000) 269.
[22] Zhou Wermin, Jiang Bohong, Liu Yang, Qi Xuan, Trans. NonFerrous Met. Soc. China 11 (2001) 555.
[23] D. Kuhlmann-Wilsdorf, in: R.M.J. Cotterill, M. Doyama, J.J. Jackson, M. Meshii (Eds.), Lattice Defects in Quenched Metals, Academic Press, New York, London, 1965, p. 269.
[24] E. Kuramoto, T. Tsutsumi, K. Ueno, M. Ohmura, Y. Kamimura, Comput. Mater. Sci. 14 (1999) 28.
[25] Dilpuneet S. Aidhy, Chenyang Lu, Ke Jin, Hongbin Bei, Yanwen Zhang, Lumin Wang, William J. Weber, Acta Mater. 99 (2015) 69.
[26] A. Kokalj, J. Mol. Graph. Modell. 17 (1999) 176.
[27] T. Egami, W. Guo, P.D. Rack, T. Nagase, Metall. Mater. Trans. A 45 (2014) 180.
[28] T. Nagase, Philip D. Rack, Joo Hyon Noh, T. Egami, Intermetallics 59 (2015) 32.
[29] Song-qin Xia, Zhen Wang, Teng-fei Yang, Young Zhang, J. Iron Steel Res. Int. 22 (2015) 879.